Clamped and sideband-resolved silicon optomechanical crystals

N.B. When citing this work, cite the original published paper.

(article starts on next page)

OPTICA

Clamped and sideband-resolved silicon optomechanical crystals

Johan Kolvik,[1,†] **Paul Burger,**[1,†] **Joey Frey,**[1] **and Raphaël Van Laer**[1,*] (iD)

[1]*Department of Microtechnology and Nanoscience (MC2), Chalmers University of Technology, Gothenburg, Sweden*
[†]*These authors contributed equally to this work.*
*raphael.van.laer@chalmers.se

Optomechanical crystals (OMCs) are a promising and versatile platform for transduction between mechanical and optical fields. However, the release from the substrate used in conventional suspended OMCs also complicates manufacturing and severely reduces thermal anchoring. This may be improved by attaching the OMCs directly to the substrate. Previous work towards such *clamped***, i.e., non-suspended, OMCs suffers from weak interaction rates and insufficient lifetimes. Here, we present a class of clamped OMCs realizing—for the first time, to our knowledge—optomechanical interactions in the resolved-sideband regime required for quantum transduction. Our approach leverages high-wavevector mechanical modes outside the continuum. We observe a record zero-point optomechanical coupling rate of $g_0/(2\pi) \approx 0.50$ MHz along with a sevenfold improvement in the single-photon cooperativity of clamped OMCs. Our devices operate at frequencies commonly used in superconducting qubits. This opens an avenue using clamped OMCs in both classical and quantum communications, sensing, and computation through scalable mechanical circuitry that couples strongly to light.** © 2023

The field of optomechanics receives great interest for applications such as sensing and microwave-to-optics transduction [1–5]. A leading class of optomechanical devices is the optomechanical crystal (OMC) [6]. In state-of-the-art suspended OMCs, the low-wavevector GHz mechanical modes are confined partly by suspending the device layer. Along with engineered bandgaps, this eliminates mechanical leakage into the substrate [6]. However, suspension also complicates manufacturing and comes at the cost of losing a channel through which heat-carrying noise phonons created by optical absorption can dissipate [7].

Confining coherent GHz phonons while letting heat-carrying noise phonons leak away fast is an understudied and challenging problem. One approach is to laterally connect a suspended OMC region with the rest of the device layer. While these two-dimensional OMCs have led to impressive results, they also require in-plane bandgaps and fine-tuning of geometry [8]. Another approach to provide thermal anchoring is to attach the OMC directly to a substrate. We call this unconventional class of OMCs

clamped. Besides reducing fabrication complexity and improving thermal anchoring, clamped devices could ease co-integration of phononic, electronic, and photonic devices, all commonly fabricated in the silicon-on-insulator (SOI) platform. Efforts along these lines have been made by using, e.g., bound states in the continuum [9] and geometrical softening [10,11]. These approaches have not yet been able to compete with the conventional suspended systems because of weaker interactions and shorter coherence times.

Here, we propose and demonstrate a new class of clamped, i.e., unreleased, OMCs. In our SOI-based OMCs, the optomechanical three-wave-mixing interaction takes places between two counterpropagating optical modes and a high-wavevector mechanical mode. We demonstrate the first clamped OMCs with mechanical frequencies exceeding their optical loss rates. This resolved-sideband condition is essential for low-noise quantum transduction between optical and mechanical fields [12]. Our new clamped OMCs have record zero-point optomechanical coupling rates. In addition, they have a thermal contact area exceeding that of their suspended counterparts. Our results provide a new path for unreleased optomechanical structures to become a competitive platform for both classical and quantum optomechanical circuits. In the following, we first outline the design process of the clamped OMCs and move on to show finite-element simulations of both photonic–phononic crystal waveguides and resonators. Finally, we present fabrication and measurement results of our devices at room temperature.

Design. A key challenge in designing clamped OMCs is avoiding excessive mechanical leakage into the substrate while keeping a high optomechanical interaction rate. In contrast to its suspended counterpart, a clamped OMC supports a continuum of states for *both* optical and mechanical waves. Here, we limit leakage from the OMC mechanical mode to substrate bulk- and surface-acoustic waves (SAWs) by exploiting large mechanical wavevectors. This enables the mechanical mode to be phase-protected from the acoustic continuum, similar to optical waveguides based on total internal reflection. Realizing strong three-wave-mixing optomechanical interactions with such high-wavevector mechanical modes requires that $k_m \approx 2k_o$, where $k_m(k_o)$ is the mechanical (optical) wavevector. This phase-matching condition is familiar from the realm of counterpropagating Brillouin interactions [13]. We illustrate the principles of phase-matching for our clamped OMCs in Fig. 1(a).
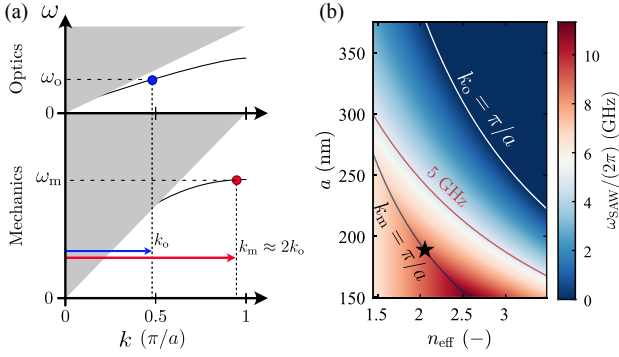
Fig. 1. (a) Phase-matching diagram for clamped and counterpropagating optomechanical interactions. The optical mode (blue) with frequency ω_o couples to a mechanical mode at ω_m. The shaded area shows the continuum that for mechanics includes both bulk- and surface-acoustic waves. Counterpropagating optical modes interact with a phase-protected mechanical mode at $k_m \approx 2k_o$ (red) whose wavevector lies outside the continuum of mechanical modes in the substrate. (b) SAW frequencies in silicon dioxide at the mechanical wavevector $k_m = 2k_o$. The optical pump has a vacuum wavelength $\lambda_0 = 1550$ nm and effective index n_{eff} and interacts with mechanics in an OMC with a unit cell with period a. Phase protection from both optical and mechanical continua is achieved for all (n_{eff}, a), where $n_{eff} > n_{cladding} = 1.45$, and $\omega_m < \omega_{SAW}$. The operating point for the presented OMC's defect unit cell is marked by a star.

For a mechanical mode with frequency ω_m to fall below the continuum, the mechanical wavevector must satisfy $k_m > \omega_m/v_{SAW}$, where v_{SAW} is the substrate SAW phase velocity. In addition, the first Brillouin zone associated with the crystal period a sets an upper bound to the set of unique wavevectors. This defines an operating window where both mechanical and optical modes are outside their continua while their three-wave-mixing is phase-matched ($k_m \approx 2k_o$). To visualize this operating window, we plot SAW frequencies for different operating points in Fig. 1(b). At a given wavevector k_m, there is a maximum frequency the OMC mechanical mode can have before entering the continuum. This upper bound for guided mechanical mode frequencies is calculated as $\omega_{SAW} = k_m v_{SAW}$, where $k_m = 2k_o$. We use optical wavevectors for a pump with effective index n_{eff} at a vacuum wavelength $\lambda_0 = 1550$ nm. In addition, we use $v_{SAW} \approx 3400$ m/s for silicon dioxide [14]. Clamped and phase-matched OMC operation with low mechanical and optical radiation losses into the substrate is accessible for all (n_{eff}, a) such that $n_{eff} > n_{cladding} = 1.45$ while also $\omega_m < \omega_{SAW}$. This analysis encourages exploration of unit cells with smaller periods a, as they provide larger operating windows.

Investigating a unit cell with period $a = 188$ nm and width $w = 643$ nm, we find a guided X-point mechanical mode at $\omega_m/(2\pi) = 5.4$ GHz (Fig. 2). At this mechanical wavevector, we calculate the SAW frequency to be $\omega_{SAW}/(2\pi) = 10.3$ GHz. This places our modes firmly outside both mechanical and optical continua. The mechanical mode profile resembles the "pinch mode" reported in [15] for suspended OMCs [Fig. 3(a)]. The mechanical motion is primarily longitudinal along the OMC, in contrast to recently explored modes [16]. The mode is guided despite the silicon device layer having faster speed of sound than the substrate. We attribute this to the unit cell's relatively large surface-to-volume ratio. This is known to reduce the effective stiffness of the structure in an effect known as geometrical softening [3,11]. We design a defect unit cell based on this mechanical mode and calculate mechanical and optical dispersion diagrams for a
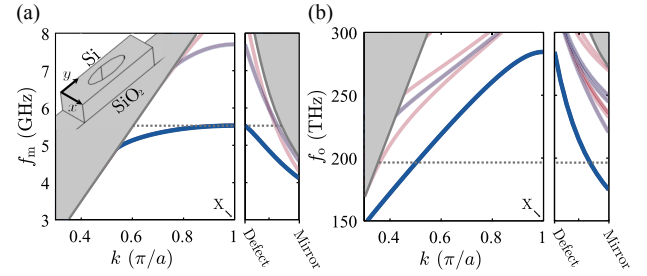

Fig. 2. (a) Mechanical and (b) optical band diagram of the OMC defect unit cell. The left inset in (a) shows the unit cell with an elliptic hole. The right insets in (a) and (b) show the X-point ($k = \pi/a$) frequencies as a function of the perturbation from defect to mirror cell. The shaded area shows the continuum modes including the SAW bands for mechanics. Blue lines denote modes with symmetry with respect to the xz plane; red lines denote modes of other symmetries. The modes of interest are solid. The horizontal dashed lines indicate the approximate OMC mode frequencies at the operating point.
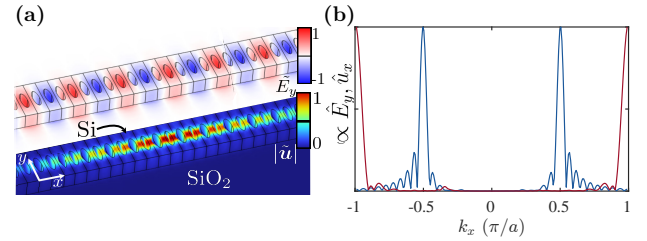

Fig. 3. (a) Optical and mechanical mode profiles. (Top) Normalized transverse optical field $\tilde{E}_y$, which largely sets the optomechanical coupling rate. (Bottom) Normalized mechanical displacement $\tilde{u}$. (b) Fourier transform of the optical field E_y (blue) and mechanical field u_x (red).

photonic–phononic crystal waveguide with periodic symmetry (Fig. 2). We choose the parameters of the unit cell such that the waveguide supports a C-band optical mode at half the mechanical wavevector. Considering counterpropagating optomechanical interactions, we calculate a unit cell zero-point optomechanical coupling rate of $g_{0,uc}/(2\pi) = 4.2$ MHz. This large coupling is mostly mediated by the moving boundary effect and is comparable to those of conventional suspended OMC defect cells [6]. We give further analysis of high-wavevector mechanics in standing-wave OMCs in Supplement 1.

To confine the waveguide mode described above in a standing-wave OMC, we design a second type of unit cell: the mirror cell. By increasing its period compared to the defect cell by about a factor of two to $a = 375$ nm, the optical and mechanical bands are pulled below the localized mode frequencies, opening a quasi-bandgap (Fig. 2). The OMC is thus assembled by transforming the defect cell in the center into the mirror cell at the cavity perimeters [17,18]. In this case, the mechanical quasi-bandgap exists for only the first half of the perturbation before the mirror cell becomes a host to the continuum modes. Yet, a mechanical quasi-bandgap lasting for only a few unit cells suffices to reflect the vast majority of the mechanical field; see Supplement 1.

A consequence of the optical mode not being at the X-point is that it is not the cavity's fundamental, but a higher-order mode. Additionally, the optical mode decays slower in the mirror transition region compared to X- or Γ-point modes. Both of these effects reduce the spatial overlap between optical and mechanical modes. We keep most of the defect unit cell's interaction strength in the
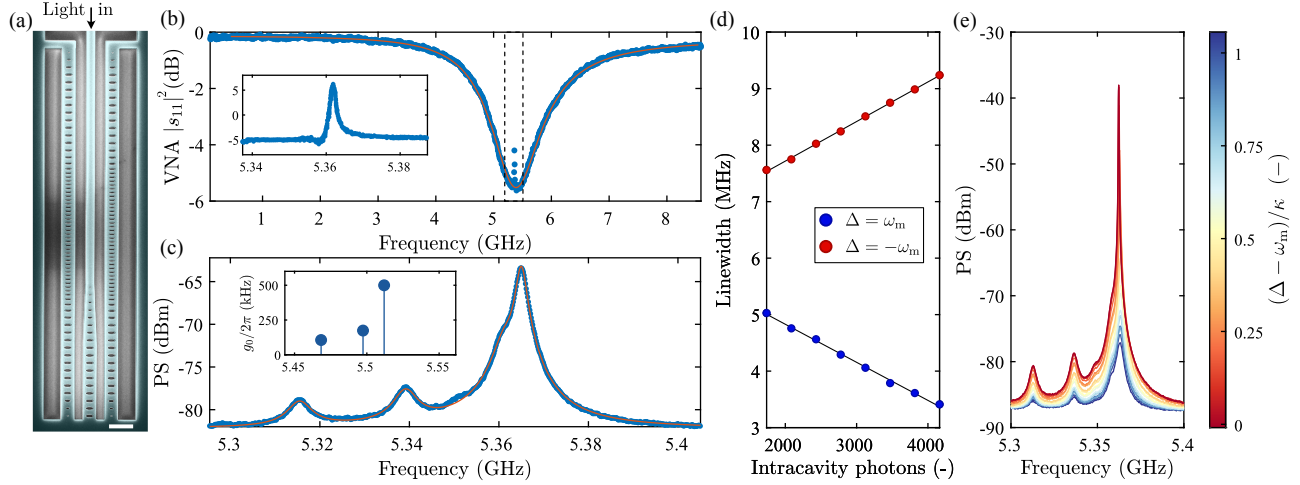
Fig. 4. Fabrication and measurement of the OMC. (a) Top-down scanning electron micrograph of two silicon clamped OMCs next to an optical bus waveguide (false color). We measure the device in reflection. Scale bar indicates 1 μm. Light enters through the center waveguide at the top of the figure and couples evanescently to the OMCs. (b) To extract the pump detuning Δ, we perform optical sideband spectroscopy of one of the OMCs measured with a vector network analyzer and a blue-detuned pump laser. The inset shows a zoomed-in view of the dashed region with higher resolution where we observe an electromagnetically induced transparency feature at the mechanical frequency. (c) The measured thermal spectrum with model fit (orange) shows a strongly coupled fundamental mechanical mode at $\omega_{\mathrm{m}}/(2\pi) = 5.365$ GHz along with two higher-order modes. (d) Effective linewidth $\gamma(1 \mp \mathcal{C})$ of the fundamental mechanical mode as a function of optical intracavity photons. This lets us extract $g_0/(2\pi) = 0.50 \pm 0.01$ MHz [12]. We carry out the experiment for both blue- and red-detuning of the pump $\Delta = \pm\omega_{\mathrm{m}}$. (e) We observe the cooperativity approaching unity and mechanical self-oscillations at 375 μW pump power injected in the bus waveguide.

full OMC by adding additional defect unit cells before starting the mirror region. Indeed, the field profiles of mechanics and optics approach the defect unit cell's fields for a clamped OMC as the number of defect unit cells N increases. While this reduces the zero-point coupling rates as $1/\sqrt{N}$, the increased interface area between a longer clamped OMC and the substrate is also expected to improve thermal anchoring. We discuss other cavity modes in Supplement 1.

At this stage, we optimize our design using a Nelder–Mead algorithm. For an optimized clamped OMC with $N = 31$ defect cells, we simulate an optical mode with $\omega_{\mathrm{o}}/(2\pi) = 195$ THz and a mechanical mode with $\omega_{\mathrm{m}}/(2\pi) = 5.511$ GHz with radiation-limited quality factors $Q_{\mathrm{o}} = 1.3 \cdot 10^6$ and $Q_{\mathrm{m}} = 3.6 \cdot 10^5$, respectively [Fig. 3(a)]. Fourier transformation of the cavity fields indicates that the phase-matching condition $k_{\mathrm{m}} \approx 2k_{\mathrm{o}}$ is met for counterpropagating optomechanical interaction [Fig. 3(b)]. The simulated zero-point optomechanical coupling of the resulting new clamped OMC design is $g_0/(2\pi) = 0.50$ MHz.

Experiments. We fabricate the clamped OMCs in 220 nm SOI and characterize the finished devices [Fig. 4(a)] at room temperature and atmospheric pressure; see Supplement 1 for details. Probing the devices with a near-infrared laser, we detect the optical resonance at $\omega_{\mathrm{o}}/(2\pi) = 193.1$ THz with a total linewidth $\kappa/(2\pi) = 1.41$ GHz and external coupling rate $\kappa_{\mathrm{e}}/(2\pi) = 600$ MHz. Next, we modulate the pump intensity and demodulate the reflected signal with a vector network analyzer [Fig. 4(b)]. We thus perform an s_{11} measurement, which is used to extract the pump detuning $\Delta = \omega_{\mathrm{L}} - \omega_{\mathrm{o}}$, where ω_{L} is the frequency of the pump laser [19]. These data are also used to confirm external optical coupling rates. In addition, we observe a strong electromagnetically induced transparency feature at the mechanical frequency [Fig. 4(b)] with a red-detuned ($\Delta = -\omega_{\mathrm{m}}$) pump and 375 μW pump power injected into the bus waveguide [20,21].

Placing the pump blue-detuned from the optical resonance at roughly $\Delta = \omega_{\mathrm{m}}$, we measure the mechanical spectrum in the reflected light with a microwave spectrum analyzer. This reveals several mechanical modes of which we show three in Fig. 4(c). The full spectrum is shown in Supplement 1. The spectral spacing and relative optomechanical coupling of the three mechanical modes qualitatively agree with simulation, and the absolute frequencies agree to within 150 MHz [Fig. 4(c) inset]. The fundamental mechanical mode frequency is at $\omega_{\mathrm{m}}/(2\pi) = 5.365$ GHz. Crucially, this puts the device operation in the resolved-sideband regime with $\omega_{\mathrm{m}}/\kappa = 3.6$. To the best of our knowledge, this is the first demonstration of a clamped OMC in this regime. We note a slight asymmetric feature in the fundamental mode [Fig. 4(c)], which we suspect is related to geometrical disorder. We move on to measure the zero-point optomechanical coupling rate by measuring the mechanical linewidth at varying optical pump powers [12] with both blue- and red-detuned pumps [Fig. 4(d)]. We find a strong zero-point optomechanical coupling rate of $g_0/(2\pi) = 0.50 \pm 0.01$ MHz and a mechanical linewidth of $\gamma/(2\pi) = 6.32$ MHz [Fig. 4(d)]. The zero-point coupling rate is in excellent agreement with simulations. The uncertainty in coupling rate g_0 stems mainly from inaccuracy in the measured on-chip powers. The single-photon cooperativity of the device is $\mathcal{C}_0 \equiv 4g_0^2/(\kappa\gamma) = 1.13 \cdot 10^{-4}$. This cooperativity exceeds that of previously measured clamped devices by a factor of about seven [9–11]. We suspect higher single-photon cooperativities are in reach at cryogenic temperatures. To highlight our device performance in relation to state of the art, we present a summary of important parameters for previous clamped work in Table 1.

Next we place the laser blue-detuned ($\Delta = \omega_{\mathrm{m}} + \kappa$) and again turn the power to 375 μW. When tuning the laser toward $\Delta = \omega_{\mathrm{m}}$, the intracavity photon number reaches $n_{\mathrm{c}} = 9.6 \cdot 10^3$. At this photon number, the cooperativity approaches unity, which we illustrate in Fig. 4(e). Here, mechanical power spectra are shown as

Table 1.   Table Comparing Clamped Optomechanical Structures on Key Parameters

Reference	*Liu et al.* (est.) [9]	*Zhang et al.* [10]	*Sarabalis et al.* [11]	**This Work**
$g_0/(2\pi)$ (kHz)	87	51	290	**500**
$\omega_{\mathrm{m}}/(2\pi)$ (GHz)	**7.5**	0.66	0.48	**5.37**
$\kappa/(2\pi)$ (GHz)	9.7	4.9	8.2	**1.4**
$\gamma/(2\pi)$ (MHz)	16	**0.6**	2.6	6.3
$\omega_{\mathrm{m}}/\kappa$ (−)	0.77	0.14	0.058	**3.6**
$\mathcal{C}_0 \equiv 4g_0^2/(\kappa\gamma)$ (−)	$2.0 \cdot 10^{-7}$	$3.5 \cdot 10^{-6}$	$1.6 \cdot 10^{-5}$	$\mathbf{1.1 \cdot 10^{-4}}$

the pump detuning is swept closer to $\Delta = \omega_{\mathrm{m}}$. When the detuning approaches the mechanical frequency, we observe self-induced oscillations in the fundamental mechanical mode—indicating $\mathcal{C} = \mathcal{C}_0 n_{\mathrm{c}} \to 1$.

In conclusion, we designed and demonstrated a new class of clamped OMCs in SOI leveraging high-wavevector mechanical modes and counterpropagating optomechanical interactions at gigahertz frequencies. To the best of our knowledge, they are the first clamped OMCs in the resolved-sideband regime—a key requirement for low-noise quantum transduction between optics and mechanics. We observe a record zero-point optomechanical coupling rate for clamped OMCs of $g_0/(2\pi) = 0.50$ MHz—in excellent agreement with simulation. Their single-photon cooperativity exceeds that of previous clamped OMCs by about an order of magnitude. We suspect that further improvements of the optomechanical overlap are in reach. We expect the clamped OMCs to show improved thermal anchoring both at room-temperature and in cryogenic environments [7,8]. Their operation relies on robust confinement of mechanical modes outside the mechanical continuum without geometrical fine-tuning. The devices may impact both classical and quantum applications; see Supplement 1. Our approach is not restricted to SOI; it is applicable to a wide range of materials and substrates. The clamped OMCs can be combined with, e.g., liquids, spins, or superconducting qubits. This opens a new avenue for scalable classical and quantum optomechanical circuits for applications in transduction, sensing, and acoustic processing of electromagnetic signals [3,22]. Mechanical systems are often seen as a universal bus. Having them clamped on a substrate while coupling strongly to light unlocks new opportunities in communication, sensing, and computation.

Disclosures.   The presented work is related to a pending patent application.

Data availability.   The datasets are available from the corresponding author upon reasonable request.

Supplemental document.   See Supplement 1 for supporting content.

REFERENCES

1. M. Mirhosseini, A. Sipahigil, M. Kalaee, and O. Painter, Nature **588**, 599 (2020).
2. W. Jiang, F. M. Mayor, S. Malik, R. Van Laer, T. P. McKenna, R. N. Patel, J. D. Witmer, and A. H. Safavi-Naeini, "Optically heralded microwave photons," arXiv, arXiv:2210.10739 (2022).
3. A. H. Safavi-Naeini, D. Van Thourhout, R. Baets, and R. Van Laer, Optica **6**, 213 (2019).
4. M. J. Weaver, P. Duivestein, A. C. Bernasconi, S. Scharmer, M. Lemang, T. C. van Thiel, F. Hijazi, B. Hensen, S. Gröblacher, and R. Stockill, "An integrated microwave-to-optics interface for scalable quantum computing," arXiv, arXiv:2210.10739 (2022).
5. S. Meesala, S. Wood, D. Lake, P. Chiappina, C. Zhong, A. D. Beyer, M. D. Shaw, L. Jiang, and O. Painter, "Non-classical microwave-optical photon pair generation with a chip-scale transducer," arXiv, arXiv:2303.17684 (2023).
6. J. Chan, A. H. Safavi-Naeini, J. T. Hill, S. Meenehan, and O. Painter, Appl. Phys. Lett. **101**, 081115 (2012).
7. S. M. Meenehan, J. D. Cohen, S. Gröblacher, J. T. Hill, A. H. Safavi-Naeini, M. Aspelmeyer, and O. Painter, Phys. Rev. A **90**, 011803 (2014).
8. H. Ren, M. H. Matheny, G. S. MacCabe, J. Luo, H. Pfeifer, M. Mirhosseini, and O. Painter, Nat. Commun. **11**, 3373 (2020).
9. S. Liu, H. Tong, and K. Fang, Nat. Commun. **13**, 3187 (2022).
10. J. Zhang, P. Nuño Ruano, X. Le-Roux, M. Montesinos-Ballester, D. Marris-Morini, E. Cassan, L. Vivien, N. D. Lanzillotti-Kimura, and C. A. Ramos, ACS Photon. **9**, 3855 (2022).
11. C. J. Sarabalis, Y. D. Dahmani, R. N. Patel, J. T. Hill, and A. H. Safavi-Naeini, Optica **4**, 1147 (2017).
12. M. Aspelmeyer, T. J. Kippenberg, and F. Marquardt, Rev. Mod. Phys. **86**, 1391 (2014).
13. B. J. Eggleton, M. J. Steel, and C. G. Poulton, *Brillouin Scattering Part 1* (Elsevier, 2022).
14. B. A. Auld, *Acoustic Fields and Waves in Solids* (Wiley, 1973), Vols. 1 & 2.
15. M. Eichenfield, J. Chan, R. M. Camacho, K. J. Vahala, and O. Painter, Nature **462**, 78 (2009).
16. X. Ma, P. K. Shandilya, and P. E. Barclay, "Semiconductor-on-diamond cavities for spin optomechanics," arXiv, arXiv:2302.04967 (2023).
17. A. H. Safavi-Naeini and O. Painter, Opt. Express **18**, 14926 (2010).
18. M. Eichenfield, J. Chan, R. Camacho, K. J. Vahala, and O. J. Painter, Opt. Express **17**, 20078 (2009).
19. J. Chan, "Laser cooling of an optomechanical crystal resonator to its quantum ground state of motion," Ph.D. thesis (California Institute of Technology, 2012).
20. S. Weis, R. Rivière, S. Deléglise, E. Gavartin, O. Arcizet, A. Schliesser, and T. J. Kippenberg, Science **330**, 1520 (2010).
21. A. H. Safavi-Naeini, T. P. M. Alegre, J. Chan, M. Eichenfield, M. Winger, Q. Lin, J. T. Hill, D. E. Chang, and O. Painter, Nature **472**, 69 (2011).
22. B. J. Eggleton, C. G. Poulton, P. T. Rakich, M. J. Steel, and G. Bahl, Nat. Photonics **13**, 664 (2019).